Research Repository UCD

Title	Open loop Kelvin probe force microscopy with single and multi-frequency excitation
Authors(s)	Collins, Liam, Kilpatrick, J. I., Weber, Stefan A. L., Rodriguez, Brian J., et al.
Publication date	2013-11-29
Publication information	Collins, Liam, J. I. Kilpatrick, Stefan A. L. Weber, Brian J. Rodriguez, and et al. "Open Loop Kelvin Probe Force Microscopy with Single and Multi-Frequency Excitation" 24, no. 47 (November 29, 2013).
Publisher	Institute of Physics
Item record/more information	http://hdl.handle.net/10197/5027
Publisher's version (DOI)	10.1088/0957-4484/24/47/475702

Downloaded 2023-10-05T14:16:07Z

The UCD community has made this article openly available. Please share how this access benefits you. Your story matters! (@ucd_oa)

© Some rights reserved. For more information

Open loop Kelvin probe force microscopy with single and multi-frequency excitation

L Collins[1,2], J I Kilpatrick[2], S A L Weber[2], A Tselev[3], I V Vlassiouk[4], I N Ivanov[3], S Jesse[3], S V Kalinin[3] and B J Rodriguez[1,2]

[1]School of Physics, University College Dublin, Belfield, Dublin 4, Ireland
[2]Conway Institute of Biomedical and Biomolecular Research, University College Dublin, Belfield, Dublin 4, Ireland
[3]Center for Nanophase Materials Sciences, Oak Ridge National Laboratory, Oak Ridge, Tennessee 37831, USA
[4]Measurement Science & System Engineering Division, Oak Ridge National Laboratory, Oak Ridge, TN 37831, USA

E-mail: sergei2@ornl.gov (S V Kalinin) and brian.rodriguez@ucd.ie (B J Rodriguez)

Abstract. Conventional Kelvin probe force microscopy (KPFM) relies on closed loop (CL) bias feedback for the determination of surface potential (SP). However, SP measured by CL-KPFM has been shown to be strongly influenced by the choice of measurement parameters due to non-electrostatic contributions to the input signal of the bias feedback loop. This often leads to systematic errors of several hundred mV and can also result in topographical crosstalk. Here, open loop (OL)-KPFM modes are investigated as a means of obtaining a quantitative, crosstalk free measurement of the SP of graphene grown on Cu foil, and are directly contrasted with CL-KPFM. OL-KPFM operation is demonstrated in both single and multi-frequency excitation regimes, yielding quantitative SP measurements. The SP difference between single and multilayer graphene structures using OL-KPFM was found to be 63 ± 11 mV, consistent with values previously reported by CL-KPFM. Furthermore, the same relative potential difference between Al_2O_3-coated graphene and Al_2O_3-coated Cu was observed using both CL and OL techniques. We observe an offset of 55 mV between absolute SP values obtained by OL and CL techniques, which is attributed to the influence of non-electrostatic contributions to the input of the bias feedback used in CL-KPFM.

1. Introduction

Nonnenmacher *et al*. [1] first reported surface potential (SP) measurements using scanning probe microscopy (SPM), adapting the concept of the macroscopic Kelvin probe [2] to utilize the high force sensitivity and lateral resolution of the atomic force microscope (AFM) [3]. Since then, Kelvin probe force microscopy (KPFM) has undergone significant advances in both sensitivity [4-7] and resolution [8-10], with a broad spectrum of configurations now available. KPFM has been applied to study a variety of materials, including organic, biological, and energy conversion and storage-related materials. For instance, KPFM has been utilized for the label-free detection of biomolecules [11, 12] and for surface photo-voltage measurements in optically active proteins [13]. Similarly, KPFM has been useful in

mapping electrostatic potential profiles across working devices [14], surface photo-voltage in photovoltaics [15-17], and charging dynamics in ferroelectric [18-20] and dielectric materials [21].

Throughout this paper we will denote open loop techniques with OL and closed loop techniques with CL. Conventional KPFM is characterized by CL bias feedback and, similar to other SPM techniques which rely on a feedback approach, is susceptible to a wide range of imaging and feedback artifacts [22-24]. An ideal feedback system minimizes the difference between an input signal (in this case the cantilever oscillation amplitude) and a setpoint (in this case 0 V as CL-KPFM is a nulling technique) by varying an output parameter (the dc bias applied to the tip or sample). We note that in CL-KPFM, the dc bias is equal to the contact potential difference (CPD) between the tip and sample when the feedback loop is performing optimally (input signal = setpoint) and where the input signal arises purely due to electrostatic contributions (*i.e.*, does not contain non-electrostatic or parasitic signals). We thus define any condition where the feedback loop is not optimized and/or where the input signal contains non-electrostatic and/or parasitic contributions as the *feedback effect* (*i.e.*, non-ideal feedback). It is widely reported that feedback effects result in SP values determined by CL-KPFM that can depend on the feedback parameters [22], the amplitude and phase reference of the excitation voltage [23,24], the tip-sample distance [25], as well as topographical crosstalk [26, 27].

In this work, we demonstrate that OL-KPFM techniques can be used to overcome the influence of feedback effects present in conventional CL-KPFM [28]. Furthermore, negating the requirement for feedback, and hence the need to apply a dc bias, makes OL-KPFM techniques a promising development with numerous potential applications including the investigation of voltage sensitive materials [29,30], time-resolved SP measurements [31,32] (OL is not limited by the bandwidth of the feedback loop), 3-dimensional-KPFM [33] (where

feedback effects in CL-KPFM introduce a distance dependence), as well as SP measurements in liquid [34-36]. Here, we demonstrate single frequency (dual harmonic (DH)) and multi-frequency (band excitation (BE)) OL-KPFM techniques, which are then directly compared *in situ* to CL-KPFM. All techniques presented are operated using the same approach (amplitude modulation (AM) in lift (dual pass) mode) to ensure an accurate comparison. Measurements are performed on single and multilayer graphene structures grown by chemical vapour deposition (CVD) on Cu foil. In addition, we compare the performance of the techniques on Al_2O_3-coated graphene/Cu foil samples.

2. Background

2.1. Electrostatic forces in voltage modulated SPM

A common feature of voltage modulated SPM techniques is the application of a dc bias, V_{dc}, which is superimposed on an ac voltage, V_{ac}, and applied between tip and sample, such that $V_{tip} = [(V_{dc} + V_{SP}) + V_{ac}\sin(\omega t)]$, where V_{SP} is the SP difference between tip and sample. The electrostatic force experienced by the tip can be separated into a static dc term, equation 1a, and two dynamic force components, equations 1b and 1c:

$$F_{dc} = -C_z'(\frac{1}{2}(V_{dc} - V_{SP})^2 + \frac{1}{4}V_{ac}^{\ 2}), \quad (1a)$$

$$F_{\omega} = -C_z'(V_{dc} - V_{SP})V_{ac}\sin(\omega t), \quad (1b)$$

$$F_{2\omega} = C_z'\frac{1}{4}V_{ac}^2\cos(2\omega t), \quad (1c)$$

where C_z' represents the capacitance gradient, which is dependent on tip/sample geometry and the dielectric properties of the tip-sample gap. Lock-in amplifiers (LIAs) are employed to measure the dynamic amplitude and phase response of the cantilever to electrical excitation. Electrostatic force microscopy (EFM) utilizes the first harmonic response (equation 1a) for charge density mapping. Thus, qualitative maps of the local electric field distribution across

the sample surface can be obtained using EFM. EFM alone, however, cannot directly provide quantitative measurements because of the difficulty in decoupling C_z' and V_{SP} information, which requires precise knowledge of the tip-sample capacitor geometry [38].

2.2. Kelvin probe force microscopy

KPFM was developed to provide quantitative measurements of SP between tip and sample and can be implemented in several ways. The measurement can be made in lift mode where the tip is excited electrically at a defined distance above a surface. Alternatively, the experiment can be performed simultaneously with surface topography acquisition using an electrical excitation at a frequency far from the mechanical excitation used for topographical feedback [39]. CL-KPFM can be operated in AM or frequency modulation (FM) modes, which are sensitive to electrostatic forces or force gradients, respectively. In AM-KPFM, the amplitude response due to an electrostatic force (F_ω) at the frequency (ω) of an applied V_{ac} is detected using a LIA. The oscillation amplitude due to the first harmonic force, which depends linearly on V_{dc}, is used as the input signal for the feedback loop that adjusts V_{dc} (which is applied to the tip or sample), thereby minimizing F_ω such that $V_{dc} = V_{SP}$. This applied bias is then used to map the local SP as the tip is scanned across the sample.

2.3. Feedback effect and topographical crosstalk in KPFM

An implicit assumption of CL-KPFM is that if the oscillation amplitude of the cantilever at the excitation frequency, ω, is minimized, the applied bias, V_{dc}, effectively compensates the electrostatic force (*i.e.*, $F_\omega = 0$) and is therefore equal to the local SP ($V_{dc} = V_{SP}$). This, however, has rarely been experimentally verified. Under the condition of $F_\omega = 0$, the measured SP can then be determined independently from measurement parameters (equation 1b). In practice, however, the interpretation of the recorded SP requires careful consideration of the influence of the instrumentation, and in particular the bias feedback loop [22, 40].

To demonstrate this, we perform a common OL spectroscopy experiment, used for determining the SP of a sample, at a single point as shown in Figure 1(a). In OL spectroscopy, the amplitude response (A_ω) to electrostatic excitation is recorded as a function of V_{dc} applied to the tip with a constant V_{ac}. The advantage of using A_ω is that it is insensitive to the reference phase of the LIA. The data was collected 50 nm above a freshly cleaved highly oriented pyrolytic graphite (HOPG) surface, using V_{ac} = 1 V at a frequency of 12.5 kHz (far from the mechanical resonance frequency, ω_0 = 65 kHz). From equation 1b, the SP is given by the tip bias (V_{dc}), which minimizes the first harmonic response, indicated in Figure 1(a) by a dashed blue line. In CL-KPFM, to allow both positive and negative SP to be measured, the input to the Kelvin feedback loop needs to be the in phase, X, (or quadrature, Y) component (*i.e.*, having a bipolar bias response) of the first harmonic response with the reference phase adjusted to maximize X (or Y). From Figure 1(a), it is clear that the minimum of A_ω is non-zero and has some finite magnitude, δ. Inspection of the graph shows that the bias at which the minimum of A_ω occurs differs from the zero crossing of X (indicated by a red dashed line). Under CL operation, the feedback loop adjusts the tip bias in order to nullify X, thus defining the SP as the X zero crossing rather than the minimum of A_ω (where $V_{dc} = V_{SP}$). Under conditions where there is a bias offset between the minimum of A_ω and the zero crossing of X, this leads to a non-quantitative absolute SP (an example of the feedback effect).

In practice, electronic offsets of the instrumentation used, parasitic signals such as capacitive coupling between ac excitation voltage and deflection output signal [23,40], along with experimental limitations, such as thermo-mechanical and electrical noise, prohibit the recorded amplitude from converging to zero (when $V_{dc} = V_{SP}$). The result of which is that absolute (*i.e.*, the real values for the system being measured) SP measurements in CL-KPFM are subject to the feedback effect and can vary typically within an instrument-dependent ~ 1

V range [23]. During CL operation, the measured SP can be further influenced by non-zero tracking errors and the choice of feedback parameters (excitation frequency, phase projection, and feedback gains) [22, 23]. Some forms of parasitic signals can be avoided. This requires careful calibration of all electronic instrumentation, shielded electronic cabling and/or active feedback compensation [23]. Otherwise, this deviation of V_{dc} from the actual V_{SP} must be taken into consideration for CL-KPFM measurements, as given by equation 2 [37],

$$V_{dc} = V_{SP} + \frac{\delta}{A_{\max}(V_{ac}C_z')}, \tag{2}$$

where $A_{max} = G(\omega,\omega_0)$ is the transfer function of the cantilever [28]. A form of equation 2 using projections into the X and Y quadrants (including their phase dependence) can be found elsewhere [23], however, here we only consider amplitude terms as they are insensitive to phase. The second term in equation 2 introduces a dependence on C_z' and V_{ac} when δ has some finite magnitude. Experimentally, this manifests in the form of a $1/V_{ac}$ dependence of the measured SP [24]. The SP recorded during a linear sweep of the V_{ac} applied to the tip is shown in Figure 1(b). For a non-zero δ, the measured SP in CL-KPFM will also become dependent on the reference phase offset [23,40].

An AM CL-KPFM potential image of single layer graphene on Cu foil is shown in Figure 1(c). As is the case in most CL-KPFM measurements, we choose to position our excitation signal at or close to ω_0 (65 kHz) to achieve improved signal to noise through resonant amplification of the electrostatic response. Operating on resonance, however, can lead to indirect crosstalk in the measured SP through bias and position dependent variations in ω_0, similar to piezoresponse force microscopy [41]. The dependence of the measured SP on the lift height, collected as the tip is scanned across a graphene/Cu boundary, is shown in Figure 1(d) and (e). A significant increase in the measured SP with increasing lift height was observed for both graphene (~ 310 mV) and the Cu foil (~ 350 mV). A nonzero δ leads to a distance dependence in the CL-KPFM measurement through contributions of C_z' as outlined

in equation 2. The observed distance dependence, however, cannot be attributed entirely to the feedback effect. Even if the tip is located directly above an area of interest, the response is not obtained solely from the area beneath the tip, but also from the interaction of the cantilever with the adjacent sample area, as shown in equation 3,

$$V_{dc} = \frac{V_{SP}^{loc} C_{loc}^{'} + V_{SP}^{avg} C_{cant}^{'}}{C_{loc}^{'} + C_{cant}^{'}} + \frac{\delta}{A_{\max}(C_{loc}^{'} + C_{cant}^{'})V_{ac}}. \quad (3)$$

Here, the effect of local (V_{SP}^{loc}, $C_{loc}^{'}$) and non-local (V_{SP}^{avg}, $C_{avg}^{'}$) contributions to the SP and the capacitance gradient are taken into account. The first two terms in equation 3 arise due to the long range nature of the electrostatic force and the interaction of the non-local (cantilever beam and tip cone) and local (tip apex) cantilever contributions [38]. However, for CL-KPFM, the relative SP or the potential difference between two points in an image (V_1 and V_2) is independent of the feedback effect, as shown by equation 4 [37],

$$(V_1 - V_2)_{measured} = (V_1 - V_2)\frac{C_{loc}^{'}}{C_{loc}^{'} + C_{cant}^{'}}. \quad (4)$$

Therefore, the change in the relative SP from -90 mV to -25 mV (Figure 1(f)) between graphene and Cu with increasing tip-sample separation is expected to be due to non-local tip-sample interactions (stray capacitance) and not feedback effects. This stray capacitance effect is a feature of all voltage modulated AFM techniques and is not confined to CL-KPFM. Nevertheless, the influence of stray capacitance on OL and CL-KPFM measurements can be minimized by adopting a FM detection scheme, which is sensitive to force gradients. In this way, FM-KPFM is only sensitive to electrostatic interactions confined to the tip apex.

Whilst FM CL-KPFM can be used to minimize such non-local contributions [32], it still suffers from the feedback effect. A major consequence of the feedback effect is topographical crosstalk, which arises from changes in C_z' due to sample topography. These

effects present significant challenges for the quantitative interpretation of contrast observed on samples with high surface roughness [26,27].

3. Open loop KPFM techniques

OL techniques present an opportunity for quantitative, crosstalk free SP imaging and have several advantages over their CL counterpart. Firstly, they simplify the experimental setup and eliminate the feedback effect present in CL-KPFM. This may prove useful for time resolved measurements [31,32], which can be limited by the bandwidth of the feedback loop in CL. Secondly, OL techniques are suitable for the characterization of voltage sensitive materials such as semiconductors, insulators, and organic and inorganic photovoltaics, where it is imperative that charge transfer between tip and sample and tip-induced band bending is suppressed [42]. Furthermore, OL techniques present a significant opportunity for extending KPFM to liquid environments for the study of electrochemical potentials at the solid-liquid interface, where electrochemical processes can dominate even at small V_{dc}.

Takeuchi *et al.* were the first to demonstrate a FM OL-KPFM technique to measure the SP of semiconducting materials in UHV [30]. Kobayashi *et al*. demonstrated the potential of an AM OL-KPFM technique for SP imaging in low molarity solutions [34-36]. Recently, DH-KPFM was demonstrated as a useful technique for investigating the electronic properties of ferroelectric materials under ambient conditions [29]. Using a similar, albeit multi-frequency approach, Guo *et al*. applied the BE method to KPFM as an OL SP mapping technique [28,43]. In the following sections, the underlying principles governing the operation of both DH-KPFM and BE-KPFM OL techniques are discussed.

3.1. Dual harmonic KPFM

In DH-KPFM, $V_{dc} = 0$. Additionally, the cantilever is excited with an ac voltage at a single drive frequency, ω, well below half ω_0 (Figure 2(a)). The resulting electrostatic force acting

on the tip produces first and second harmonic responses of the cantilever, as shown in Figure 2(a) and described by equation 5:

$$A_{\omega} = G_{\omega}\frac{|F_{\omega}|}{k} = G_{\omega}\left|\frac{\partial C}{\partial z}(V_{SP})\right|\frac{V_{ac}}{k}, \tag{5a}$$

$$A_{2\omega} = G_{2\omega}\frac{|F_{2\omega}|}{k} = G_{2\omega}\left|\frac{\partial C}{\partial z}\right|\frac{V_{ac}^{2}}{4k}, \tag{5b}$$

$$V_{SP} = \frac{A_{\omega}\cos(\varphi_{\omega})}{A_{2\omega}}\frac{V_{ac}}{4X_{gain}}, \tag{5c}$$

where G_{ω} and $G_{2\omega}$ are the gains due to the cantilever transfer function at ω and 2ω respectively, and $X_{gain} = G_{\omega}/G_{2\omega}$. DH-KPFM can be used to determine V_{SP} for a given V_{ac} with knowledge of X_{gain}, as described by equation 5c. The polarity of V_{SP} is given by the phase (φ_{ω}) of the cantilever response at ω. X_{gain} can be found by measuring the first harmonic response with excitation at ω and 2ω consecutively to obtain G_{ω} and $G_{2\omega}$. Resonance tracking techniques such as dual frequency resonance tracking [44] and BE techniques [45] can be configured to perform OL-KPFM measurements on the mechanical resonance or higher eigenmodes, while overcoming complications in determining the effective X_{gain} whilst scanning due to changes in ω_0 and the quality factor, Q.

3.2. Band excitation KPFM

The BE method is an alternative to traditional LIA based techniques. BE uses a digital signal with predefined amplitude and phase content across a continuous range of frequencies. The synthesized signal is inverse Fourier transformed to generate a signal in the time domain that can be used to excite the cantilever, as shown in Figure 2(b). The response can then be detected in a chosen frequency band using high-speed data acquisition methods. The ratio of the Fourier transform of the response and excitation signals yields the transfer function of the

cantilever, *i.e.*, the segment of the response–frequency curve in the vicinity of the mechanical resonance. The behaviour of the cantilever can be approximated by a simple harmonic oscillator (SHO) and thereby described by three parameters: ω_0, amplitude at the resonance, $A(\omega_0) = A_0$, and Q, as given by equation 6:

$$A(\omega) = \frac{A_{\max}\omega_0^2}{\sqrt{(\omega^2 - \omega_0^2)^2 + (\omega\omega_0 / Q)^2}}, \qquad (6a)$$

$$\varphi(\omega) = \tan^{-1}\left(\frac{\omega\omega_0 / Q}{\omega^2 - \omega_0^2}\right). \qquad (6b)$$

Maps of ω_0, A_0, and Q are then de-convoluted from the measurement and stored as images. The BE method has previously been applied to KPFM. Guo *et al.* demonstrated two configurations: firstly, OL BE-KPFM [28], a bias spectroscopy measurement where the 4D amplitude response of the cantilever vs. frequency, bias, and position was collected; and, secondly, half harmonic band excitation (HHBE) -KPFM [43], where two 3D BE data sets corresponding to the first and second harmonic amplitudes as a function of frequency and position at fixed tip dc biases were acquired. The operation of HHBE-KPFM is described in detail in Figure 3. In this technique the cantilever is electrically excited in a frequency band with a central frequency positioned at ω_0 (Figure 3(a)), and the response is recorded for the same frequency band. The second harmonic response of this excitation is located in a band centred at twice the excitation frequencies ($2\omega_0$), falling outside of the cantilever resonance and detection band. To detect the second harmonic response, a subsequent measurement is performed where the cantilever is excited across a band centred at half the resonance frequency ($\omega_0/2$), which is termed as half band excitation (HBE) [43]. Thus a second harmonic response is generated in the frequency band around the resonance peak. In HHBE-KPFM, the BE and HBE excitations are applied sequentially for each image pixel. In this manner, first and second harmonic components of response can be compared directly since

they fall within the same band of the cantilever transfer function and $X_{gain} = G_{\omega}/G_{2\omega} = 1$ as discussed by Guo *et al*. [43].

4. Materials and Methods

All measurements were performed using Pt–Ir-coated cantilevers (Nanosensors, PPP-EFM) with nominal resonant frequency and stiffness of 65 kHz and 2.8 N/m, respectively. A commercial AFM (Asylum Research, MFP-3D) was used. Measurements were conducted in lift mode, where the topography was recorded in AM mode during the first pass and the KPFM measurements took place at a lift height of 50 nm during the second pass, unless otherwise stated. A LIA (Zurich Instruments, HF2LI) was used to control the V_{ac} applied to the tip and to monitor the cantilever response. For all DH-KPFM measurements, V_{ac} = 2 V at a frequency of 12.5 kHz, which is less than half of ω_0 = 65 kHz. BE-KPFM was implemented using NI-5122 and NI-5412 cards (National Instruments) controlled by custom Matlab software (MathWorks). An excitation signal with an amplitude of 2 V with a centre frequency at 65.75 kHz and bandwidth of 10 kHz with 24 bins per band was applied to the tip. Graphene was fabricated by CVD on Cu foil (Alfa Aesar, #13382) as described in detail elsewhere [46,47]. Deposition of Al_2O_3 layers on graphene coated substrates was performed using an Oxford Instruments FlexAL system at a substrate temperature of 150℃ with remote oxygen plasma activation. Raman spectra of graphene samples were collected in the back scattering configuration using a Renishaw 1000 system with a HeNe laser (632.8 nm). The line laser excitation and scattering light collection was through a 50 x objective using an integration time of 10 s and static mode with a 1800 g/mm grating positioned at 2670 cm^{-1}.

5. Results and Discussion

5.1. KPFM and Raman spectroscopy of graphene

The CL-KPFM SP of a graphene film grown by CVD on Cu foil is shown in Figure 4(a). The presence of graphene layers could not be determined by thickness changes in the topography (not shown), primarily due to the high surface roughness (~ 490 nm RMS) of the underlying Cu foil. In CL-KPFM, however, pronounced contrast in SP between the materials was observable, making identification of hexagonal structures possible. It has previously been shown, using scanning electron microscopy and Raman spectroscopy, that hexagonal single layer graphene was formed under these conditions [46]. Furthermore, multilayer structures with different stacking orders are expected to be present. In Figure 4(a), regions of higher SP close to the centre of the hexagon structure were observed in CL-KPFM. Raman spectroscopy was used to investigate the presence of single and multilayer graphene (Figure 4(b)). The spectrum features low frequency first order resonance D- and G-bands and a high frequency 2D (G′) band resulting from double resonance processes [48]. As the number of graphene layers increases, the 2D band is expected to be shifted towards higher frequencies coinciding with peak broadening (*i.e.*, increased fill width at half maximum (FWHM)) and decreased intensity [49]. This 2D peak is composed of four components, which become apparent in two or more layer structures. These peaks have different phonon symmetries and show inter-dependent response to stimuli [50]. Thus, upshift in the 2D position may be considered as a reduction in the intensity of P11 and P12 and an increase in the intensity of P21 and P22 components of the 2D-band. Moreover, in graphene bilayers, the intensity of the G and 2D bands depends on the bilayer twisting angle (and the excitation laser frequency), reaching a maximum at a 10.5° twist for 632.8 nm excitation [51]. In our data, the shape of the 2D band with pronounced P11 and P12 bands and weaker P21 and P22 components suggest that it is mostly composed of single layer graphene. The 2D peak was fitted using a Lorentzian function to extract FWHM, intensity, and peak position. An analysis of the peak shape for a line-Raman scan across the graphene crystal is shown in Figure 4(c). The peak

position shifted by ~ 10 cm^{-1} to lower frequencies compared to the peak position of a single layer graphene (2685 cm^{-1}). The FWHM of the band decreased from 50 cm^{-1} to 30 cm^{-1} for the centre of the graphene crystal while the 2D band intensity increased by a factor of 4 in the same region. These Raman signatures are consistent with the presence of a single graphene crystal with a smaller graphene crystal residing at its centre being twisted with respect to the bottom layer by roughly 10°. A higher SP of 128 ± 10 mV was observed on multilayer graphene than the surrounding single layer graphene, which can be understood in terms of a shift of the Fermi level with respect to the Dirac point as a result of substrate induced doping and interlayer screening [52,53]. While we are confident that changes observed in both Raman spectroscopy and CL-KPFM measurements are related to the changes in the electronic structure due to stacking of graphene layers, unambiguous determination of layer thickness is beyond the scope of this work.

5.2. DH-KPFM

The first and second harmonic amplitude response images collected in DH-KPFM are depicted in Figure 5(a) and (b). The first harmonic map, which includes charge terms, shows similar hexagonal graphene structures as those observed in Figure 4(a). The second harmonic response, which is related to C_z', is relatively featureless, showing only small variations related to surface roughness. This second harmonic channel can be useful in mapping local polarization forces and dielectric properties of the sample which, with careful consideration, can be made quantitative [54-57]. The phase of the first harmonic map (Figure 5(c)) was used to determine the polarity of the SP. A phase inversion of 180° occurs as the local tip-sample SP changes in polarity. The resulting SP (Figure 5(d)) was determined using equation 5c. The frequency gain was experimentally determined by the acquisition of force curves while driving at ω and 2ω, consecutively. The ratio of first harmonic response recorded at ω and

2ω gave an average X_{gain} of 0.85 ± 0.01 which was used in equation 5c for determination of the resulting SP (Figure 5(d)).

Similar to the CL-KPFM measurements, large single-layer regions with lower SP can be distinguished from the Cu foil, with a SP in the centre of the hexagonal structure attributed to multilayer formation. The mean and standard deviation of the SP was determined in the square regions outlined in Figure 5(d) for the single layer (18 ± 8 mV) and multilayer (-45 ± 7 mV) regions. The potential difference between single and multilayer graphene was found to be 63 ± 11 mV. These values are in agreement within experimental error with those reported by Ziegler *et al*. who observed a variation of ~ 68 mV between single and bilayer graphene mechanically exfoliated and resting on SiO_2 [53].

5.3. HHBE-KPFM

Using the same principles as DH-KPFM (equation 5c), the SP can be determined using HHBE-KPFM from the first and second harmonic amplitude (Figure 6(e) and (f)). In agreement with both KPFM and DH-KPFM, single layer graphene from a different area on the graphene/Cu sample was found by HHBE-KPFM to be at a lower SP compared to that of the Cu foil (Figure 6(d)). As HHBE-KPFM is operated around resonance, it is possible to extract and plot ω_0, Q, and A_0 for A_ω and $A_{2\omega}$ (as shown in Figure 6(b), (c), (e) and (f) respectively) [58]. In this way, BE-KFPM combines features of both AM and FM-KPFM through measurement of the full cantilever response. Thus, frequency shifts due to conservative tip-sample interactions and changes in Q, due to dissipative interactions, can be identified. In Figure 6(b) and (c), small changes in ω_0 (< 35 Hz) and Q (< 6 % relative variation) are evident between Cu and graphene surfaces. Changes in ω_0 correspond to local topographical variations and are related to C_z'. Although charge density information is expected to be present in this channel it is possible that the tip was too far above the surface (~ 50 nm) to be sensitive to changes in the local force gradient, explaining why FM-KFPM is

typically not operated in lift mode. The small changes in Q between graphene and Cu, while interesting, are difficult to interpret due to possible parameter coupling during SHO fitting, which is especially pronounced for small amplitudes where instrument noise may be significant [28].

In KPFM measurements, it is common to perform dynamic measurements where changes in the SP are induced by electrical, chemical or optical stimulus of the sample. Here, to explore the effect of surface modification on graphene structure and SP, a 4 nm thick layer of Al_2O_3 was deposited using atomic layer deposition. All three techniques described in previous sections were performed on a single layer graphene crystal to allow direct comparison of techniques.

5.4. Comparison of techniques

In order to compare SPs recorded using OL and CL techniques, each technique was used to measure the SP of the same single layer graphene structure. Al_2O_3 coating had the effect of reversing the graphene-substrate SP contrast. This contrast inversion was observed in all three modes of operation (Figure 7). The SP values recorded by DH-KPFM and HHBE-KPFM coincided, whereas an offset of ~ 55 mV was recorded between OL and CL techniques (Figure 7(d)). The measurements, which were all performed at the same lift height, were repeated in different orders to ensure the offset was systematic and not a result of instrument drift. The main difference between experimental setups, aside from small instrument offsets (<< 55 mV), was the feedback loop employed during CL operation. Thus, we attribute the measured offset to the previously described feedback effect. All techniques recorded a SP difference of ~ 120 mV between the Al_2O_3-coated graphene and the Al_2O_3-coated Cu foil (Figure 7(e)). This is expected from equation 4, since the feedback effect does not influence the ability of CL-KPFM to make relative SP measurements.

6. Summary

We have investigated the SP of single and multilayer graphene using OL-KPFM with single and multi-frequency excitation schemes. We observed an increase in the SP between single and multilayer formations, in agreement with previous studies. The requirement for bias feedback in CL-KPFM means that absolute SP measurements are often difficult to attain (*i.e.*, the real physical value cannot be easily de-convolved from the measurement), and generally, only relative measurements (*i.e.*, between the graphene and the substrate) are routinely attainable. OL-KPFM techniques overcome the requirement for bias feedback, and hence the application of a dc bias, for quantitative determination of the SP and have the added advantage of being applicable in liquid environments. Furthermore, the BE approach can be used to overcome complications relating to the cantilever transfer function, as each harmonic can be recorded in the same frequency space, and potentially allows contributions to conservative and dissipative forces in a KPFM experiment to be identified simultaneously.

Acknowledgments

This publication has emanated from research conducted with the financial support of UCD Research. The research was conducted primarily at the Center for Nanophase Materials Sciences, which is sponsored at Oak Ridge National Laboratory by the Scientific User Facilities Division, Office of Basic Energy Sciences, U.S. Department of Energy (CNMS2012-036). JK acknowledges support provided by NANOREMEDIES, which is funded under the Programme for Research in Third Level Institutions Cycle 5 and co-funded by the European Regional Development Fund. SW acknowledges support from the Alexander von Humboldt Foundation. The authors are grateful to Zurich Instruments for their support. Some of the measurements were performed on equipment funded by Science Foundation Ireland (SFI07/IN1/B931).

References

1. Nonnenmacher M, O'Boyle M P and Wickramasinghe H K 1991 *Appl. Phys. Lett.* **58** 2921-3
2. Kelvin L, Fitzgerald G and Francis W 1898 *Phil. Mag.* **46** 82-120
3. Binnig G, Quate C F and Gerber C 1986 *Phys. Rev. Lett.* **56** 930-3
4. Sommerhalter C, Matthes T W, Glatzel T, Jager-Waldau A and Lux-Steiner M C 1999 *Appl. Phys. Lett.* **75** 286-8
5. Sommerhalter C, Glatzel T, Matthes T W, Jäger-Waldau A and Lux-Steiner M C 2000 *Appl. Surf. Sci,* **157** 263-8
6. Zerweck U, Loppacher C, Otto T, Grafström S and Eng L M 2005 *Phys. Rev. B* **71** 125424
7. Ziegler D and Stemmer A 2011 *Nanotechnology* **22** 075501
8. Fujihira M 1999 *Annu. Rev. Mater. Sci.* **29** 353-80
9. Zerweck U, Loppacher C, Otto T, Grafström S and Eng L 2007 *Nanotechnology* **18** 084006
10. Sadewasser S, Jelinek P, Fang C K, Custance O, Yamada Y, Sugimoto Y, Abe M and Morita S 2009 *Phys. Rev. Lett.* **103** 266103
11. Sinensky A K and Belcher A M 2007 *Nat. Nanotech.* **2** 653-9
12. Leung C, Kinns H, Hoogenboom B W, Howorka S and Mesquida P 2009 *Nano Lett.* **9** 2769-73
13. Knapp H F, Mesquida P and Stemmer A 2002 *Surf. Interface Anal.* **33** 108-12
14. Tanimoto M and Vatel O 1996 *J. Vac. Sci. Technol. B* **14** 1547-51
15. Loppacher C, Zerweck U, Teich S, Beyreuther E, Otto T, Grafstrom S and Eng L M 2005 *Nanotechnology* **16** S1-S6
16. Liscio A, De Luca G, Nolde F, Palermo V, Müllen K and Samorì P 2008 *J. Am. Chem. Soc.* **130** 780-1
17. Berger R, Domanski A L and Weber S A L 2013 *Eur. Polym. J.* **49** 1907-15
18. Shvebelman M M, Agronin A G, Urenski R P, Rosenwaks Y and Rosenman G I 2002 *Nano Lett.* **2** 455-8
19. Son J, Kim B G, Kim C and Cho J 2004 *Appl. Phys. Lett.* **84** 4971
20. Kim Y, Park M, Bühlmann S, Hong S, Kim Y K, Ko H, Kim J and No K 2010 *J. Appl. Phys.* **107** 054103
21. Cunningham S, Larkin I A and Davis J H 1998 *Appl. Phys. Lett.* **73** 123
22. Jacobs H, Knapp H and Stemmer A 1999 *Rev. Sci. Instrum.* **70** 1756
23. Mélin T, Barbet S, Diesinger H, Théron D and Deresmes D 2011 *Rev. Sci. Instrum.* **82** 036101--3
24. Wu Y and Shannon M A 2006 *Rev. Sci. Instrum.* **77** 043711
25. Liscio A, Palermo V, Müllen K and Samorì P 2008 *J. Phys. Chem. C* **44** 17368-17377
26. Efimov A and Cohen S R 2000 *J. Vac. Sci. Technol*., A **18** 1051-1055
27. Okamoto K, Sugawara Y and Morita S 2002 *Appl. Surf. Sci*., **188** 381-5
28. Guo S, Kalinin S V and Jesse S 2012 *Nanotechnology* **23** 125704-25713
29. Collins L, Kilpatrick J I, Bhaskaran M, Sriram S, Weber S A L, Jarvis S P and Rodriguez B J 2012 Applications of Ferroelectrics held jointly with 2012 European Conference on the Applications of Polar Dielectrics and 2012 International Symp Piezoresponse Force Microscopy and Nanoscale Phenomena in Polar Materials (ISAF/ECAPD/PFM), 2012 Intl Symp (IEEE) 1-4
30. Takeuchi O, Ohrai Y, Yoshida S and Shigekawa H 2007 *Jpn. J. Appl. Phys., Part 1* **46** 5626
31. Coffey D C and Ginger D S 2006 *Nat. Mat.* **5** 735-740
32. Strelcov E, Jesse S, Huang Y L, Teng Y C, Kravchenko I I, Chu Y H and Kalinin S V 2013 *ACS Nano* **7** 6806-15
33. Bayerl D J and Wang X 2012 A*dv. Func. Mat.* **22** 652-660
34. Kobayashi N, Asakawa H and Fukuma T 2010 *Rev. Sci. Instrum.* **81** 123705
35. Kobayashi N, Asakawa H and Fukuma T 2011 *J. Appl. Phys.* **110** 044315
36. Kobayashi N, Asakawa H and Fukuma T 2012 *Rev. Sci. Instrum.* **83** 033709
37. Kalinin S V and Bonnell D A 2001 *Phys. Rev. B* **63** 125411

38. Cherniavskaya O, Chen L W, Weng V, Yuditsky L and Brus L E 2003 *J. Phys. Chem. B* **107** 1525-31
39. Leung C, Maradan D, Kramer A, Howorka S, Mesquida P and Hoogenboom B W 2010 *Appl. Phys. Lett.* **97** 203703
40. Diesinger H, Deresmes D and M´elin T 2012 *Kelvin Probe Force Microscopy* vol 48, ed S Sadewasser and T Glatzel (Berlin: Springer) pp 25–44
41. Jesse S, Guo S, Kumar A, Rodriguez B J, Proksch R and Kalinin S V 2010 *Nanotechnology* **21** 405703
42. Yoshida S, Kikuchi J, Kanitani Y, Takeuchi O, Oigawa H and Shigekawa H 2006 *e-J. Surf. Sci. Nanotechnol.* **4** 192-6
43. Guo S, Kalinin S V and Jesse S 2012 *Appl. Phys. Lett.* **100** 063118
44. Rodriguez B J, Callahan C, Kalinin S V and Proksch R 2007 *Nanotechnology* **18** 475504
45. Jesse S, Kalinin S V, Proksch R, Baddorf A and Rodriguez B 2007 *Nanotechnology* **18** 435503
46. Vlassiouk I, Regmi M, Fulvio P, Dai S, Datskos P, Eres G and Smirnov S 2011 *ACS Nano* **5** 6069-76
47. Vlassiouk I, Fulvio P, Meyer H, Lavrik N, Dai S, Datskos P and Smirnov S 2013 *Carbon* **54** 58–67
48. G and Saito R 2010 *Nano Lett*. **3** 751-8
49. Ferrari A, Meyer J, Scardaci V, Casiraghi C, Lazzeri M, Mauri F, Piscanec S, Jiang D, Novoselov K and Roth S 2006 *Phys. Rev. Lett.* **97** 187401
50. Malard L, Pimenta M, Dresselhaus G and Dresselhaus M 2009 *Physics Reports* **473** 51-87
51. Havener R W, Zhuang H, Brown L, Hennig R G and Park J 2012 *Nano Lett*. **6** 3162-7
52. Yu Y J, Zhao Y, Ryu S, Brus L E, Kim K S and Kim P 2009 *Nano Lett.* **9** 3430-4
53. Ziegler D, Gava P, Güttinger J, Molitor F, Wirtz L, Lazzeri M, Saitta A, Stemmer A, Mauri F and Stampfer C 2011 *Phys. Rev. B* **83** 235434
54. Fumagalli L, Ferrari G, Sampietro M and Gomila G 2009 *Nano Lett.* **9** 1604-8
55. Fumagalli L, Esteban-Ferrer D, Cuervo A, Carrascosa J L and Gomila G 2012 *Nat. Mat.* **11** 808-16
56. Lucchesi M, Privitera G, Labardi M, Prevosto D, Capaccioli S and Pingue P 2009 *J. Appl. Phys*. **105** 054301
57. Nguyen H K, Labardi M, Capaccioli S, Lucchesi M, Rolla P and Prevosto D 2012 *Macromolecules* **45** 2138-2144
58. García R and Herruzo E T 2012 *Nat. Nanotech.* **7** 217-26

Figure Captions

Figure 1. (a) Electrostatically excited cantilever response over a HOPG surface as a function of V_{dc} showing the amplitude, R, and the in phase component, X (V_{ac} = 1 V, ω = 12.5 kHz, lift height ~ 50 nm). (b) SP as a function of V_{ac} recorded with CL-KPFM. (c) SP image of graphene deposited on Cu foil (scale bar 5 μm, vertical scale -240 to -40 mV). (d) Recorded SP over area marked with dashed black line in (c) as a function of lift height (5 nm – 1 μm) (scale bar 2 μm, vertical scale ± 250 mV). (e) Corresponding cross-sections of a graphene/Cu interface at different lift heights. (f) Tip-sample distance dependence of the relative SP between graphene and Cu.

Figure 2. Schematic describing (a) single frequency and (b) BE excitation schemes and responses. In DH-KPFM (a), the cantilever is driven with a simple sinusoidal function with a fixed frequency, such that the response does not fall near the mechanical resonance peak of the cantilever transfer function. For BE (b), an excitation signal with a predetermined amplitude density in a frequency band around the cantilever resonance frequency is selected. This excitation is inverse Fourier-transformed into the time domain and used to drive the cantilever. The response of the cantilever to this signal is Fourier-transformed to reconstruct the cantilever transfer function.

Figure 3. Schematic of HHBE-KPFM operation. (a) BE is performed with electrical excitation in a band having a central frequency at ω_0, the first harmonic response is recorded within the same band but the second harmonic lies outside the detection bandwidth at $2\omega_0$. (b) HBE ($\omega_0/2$) is performed sequentially and the second harmonic response is recorded in the frequency (doubled) band around ω_0. In this way, the first and second harmonic responses are in the same frequency band.

Figure 4. KPFM and Raman characterization of single and multilayer graphene samples. (a) CL-KPFM SP image (scale bar 5 μm, vertical scale 350 to 550 mV). (b) Raman spectra of graphene showing band assignment. (c) Raman line data from approximately the same region as the SP cross-section indicating the 2D peak intensity (top) and position (middle), and SP cross-section taken from area marked with a black dashed line in (a) (bottom).

Figure 5. DH-KPFM imaging of single and multilayer graphene. (a) First (scale bar 5 μm, vertical scale ± 510 a.u.) and (b) second (vertical scale ± 500 a.u.) harmonic response map of graphene on Cu foil. (c) First harmonic phase used to determine the polarity of the SP (vertical scale ± 90°). (d) SP determined from (a-c) using V_{ac} = 2 V and X_{gain} = 0.85. White boxes indicate areas used for the determination of average the single (dashed) and multilayer (solid) SP (vertical scale -50 to 250 mV).

Figure 6. HHBE-KPFM maps of single layer graphene on Cu foil. (a) Topography (scale bar 5 μm, vertical scale ± 510 nm), (b) cantilever frequency shift (vertical scale ± 35 Hz), and (c) quality factor maps (vertical scale ± 7 corresponding to < 6 % relative variation). (d) SP (vertical scale 200 to 500 mV). (e) First (vertical scale ± 510 a.u.) and (f) second (vertical scale ± 18 a.u.) harmonic BE responses.

Figure 7. SP images of a single hexagonal graphene layer collected with different techniques. (a) KPFM, (b) DH-KPFM, and (c) HHBE-KPFM images (scale bar 2 μm, vertical scale = 200 mV, offset = +135 mV for all images). Bar chart showing (d) SP (mean ± std. dev.) for

graphene and Cu and (e) the SP difference (mean ± std. dev.) measured using CL-KFPM, DH-KPFM, and HHBE-KPFM.

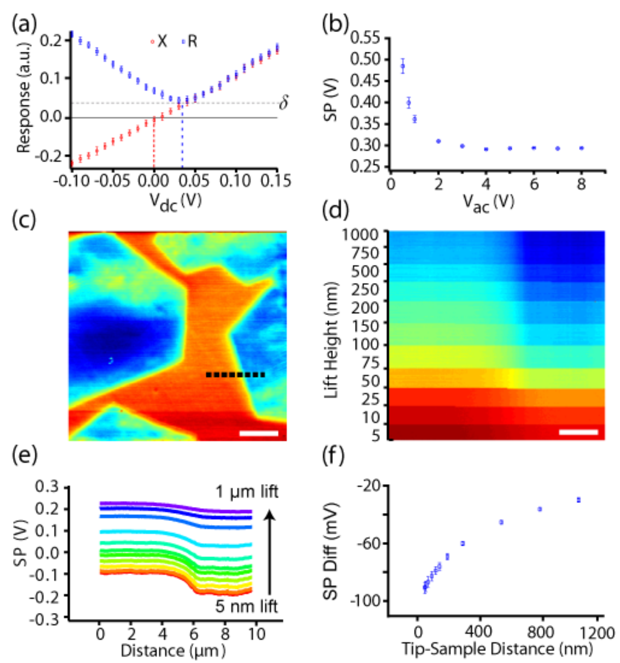

Figure 1. L. Collins *et al*.

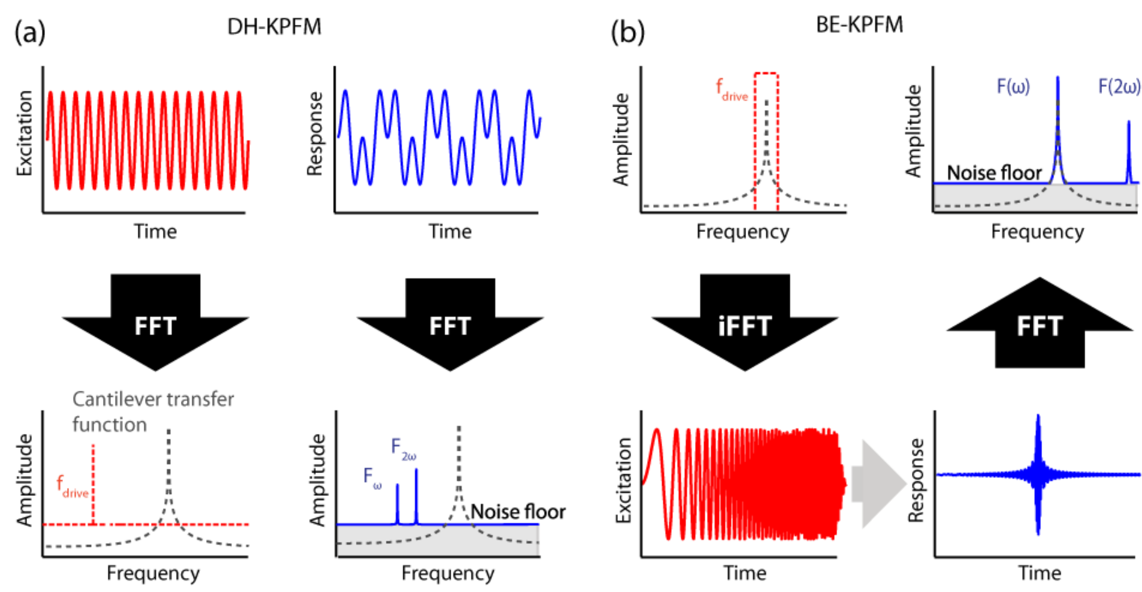

Figure 2. L. Collins *et al*.

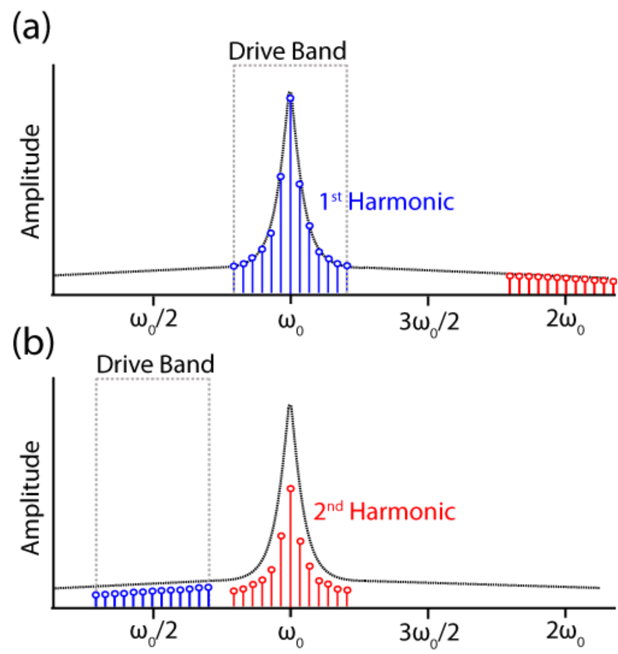

Figure 3. L. Collins *et al*.

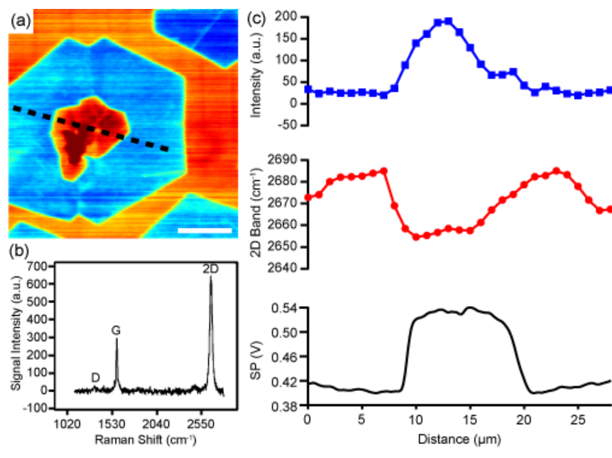

Figure 4. L. Collins *et al*.

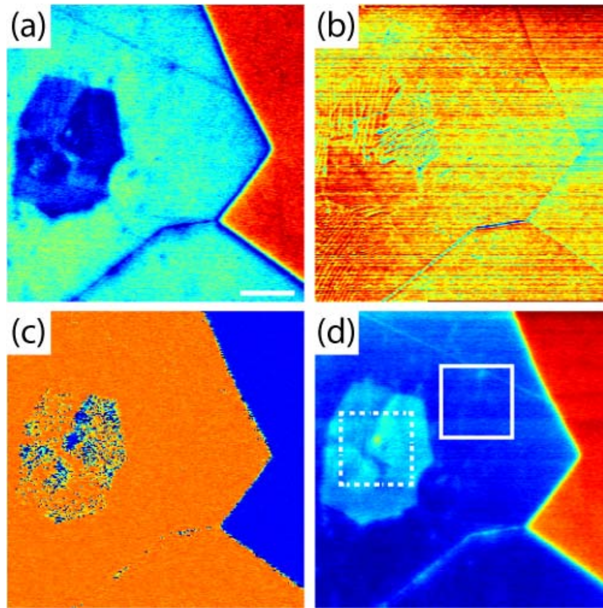

Figure 5. L. Collins *et al*.

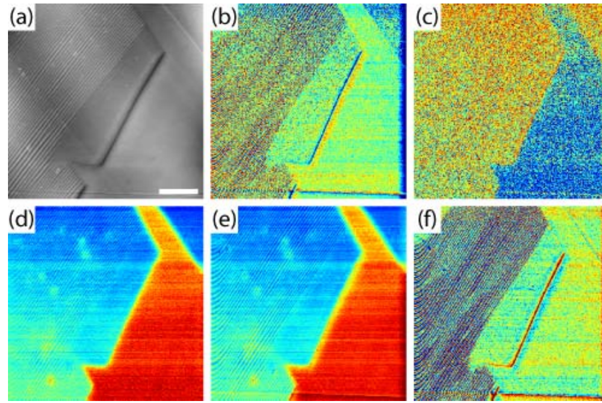

Figure 6. L. Collins *et al*.

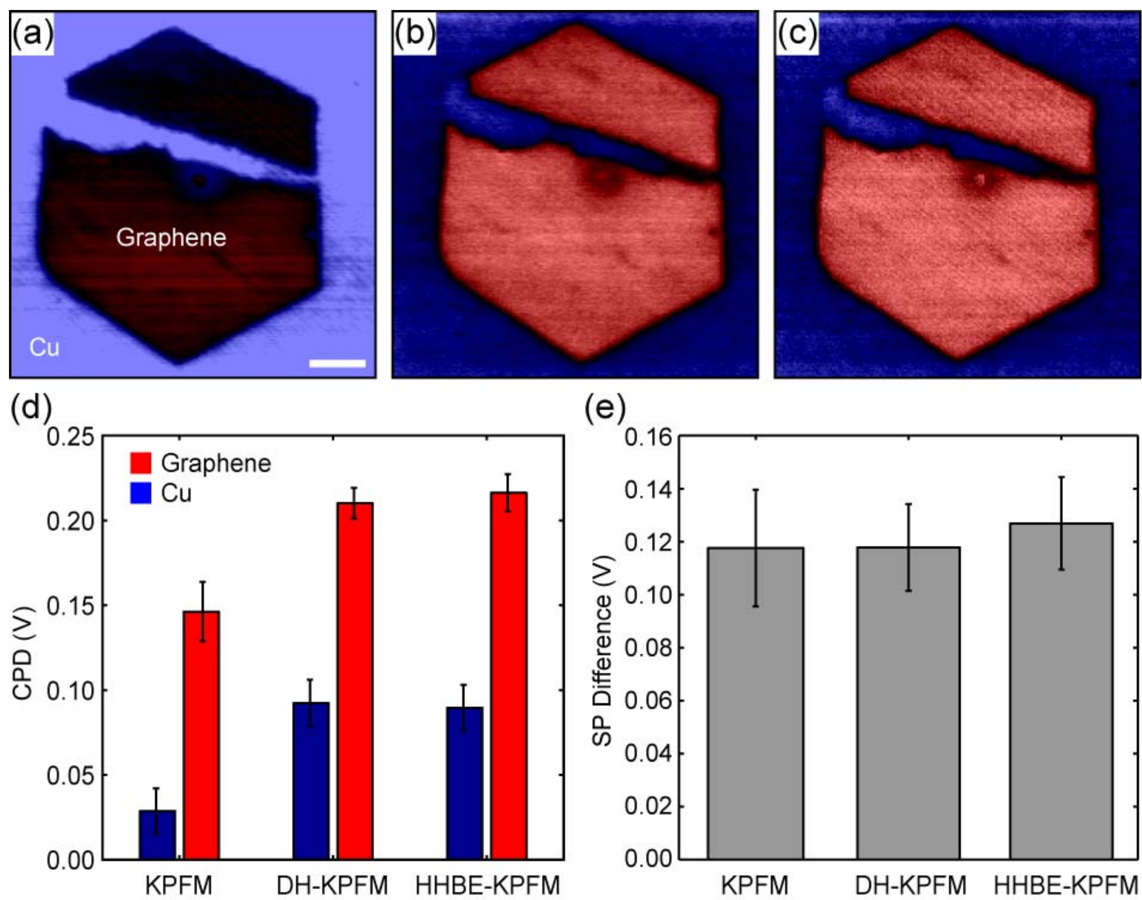

Figure 7. L. Collins *et al*.